Journal of Materials Chemistry A

PAPER

View Article Online
View Journal | View Issue

Cite this: J. Mater. Chem. A, 2014, 2, 16474

Pd-decorated three-dimensional nanoporous Au/Ni foam composite electrodes for H_2O_2 reduction

Xi Ke,[a] Yantong Xu,[a] Changchun Yu,[b] Jie Zhao,[b] Guofeng Cui,*[a] Drew Higgins,[cd] Zhongwei Chen,[d] Qing Li,[c] Hui Xu[c] and Gang Wu[ce]

Received 23rd May 2014
Accepted 8th August 2014

DOI: 10.1039/c4ta02586e

www.rsc.org/MaterialsA

Nanoporous gold (NPG) films were fabricated on Ni foam substrates *via* a two-step procedure which involves electrodeposition of Au–Sn alloy films on the Ni foam surface, followed by selectively leaching the Sn component through a chemical dealloying process. Pd nanoparticles were then electrochemically deposited on the NPG/Ni foam electrode. The morphology of the Pd-decorated NPG/Ni foam composite electrode (Pd@NPG/Ni foam) was characterized by scanning electron microscopy (SEM). The catalytic activity of the Pd@NPG/Ni foam composite electrode toward H_2O_2 electroreduction in acid media was evaluated by means of linear scan voltammetry and chronoamperometry. The Pd@NPG/Ni foam composite electrode exhibited high activity and excellent stability for the H_2O_2 electroreduction, generating a current density of 178 mA cm^{-2} at 0 V in a 0.5 M H_2SO_4 + 0.6 M H_2O_2 electrolyte, in comparison to 98 mA cm^{-2} on the Pd@Ni foam electrode and 36 mA cm^{-2} on the NPG/Ni foam electrode. The developed three-dimensional (3D) hierarchical porous Pd@NPG/Ni foam can therefore be considered as a promising type of electrode for fuel cell applications.

1. Introduction

Hydrogen peroxide (H_2O_2) has been used as an oxidant in direct liquid fuel cells such as sodium borohydride–H_2O_2 and hydrazine–H_2O_2 fuel cells, which are being developed as unique power sources for air-free conditions such as those encountered in underwater and outer space applications.[1,2] The replacement of O_2 by H_2O_2 as the oxidant in fuel cells can provide faster reduction kinetics and higher power density,[3] although these performance parameters are directly governed by the electrocatalytic reduction rate of H_2O_2 at the cathode.[4] As such, considerable efforts have been devoted to the development of efficient electrocatalysts for H_2O_2 reduction.[5–18] These include the use of noble metals (*e.g.*, Pt,[5] Pd,[6] Au,[8,9] Ag[10] and their alloys[11,12]) and noble-metal-free transition metal oxides (*e.g.*, Co_3O_4[13,14] and CuO[15]) as well as the combinations consisting of both constituents.[17] Among these, noble metals exhibit the highest activity and the most reliable performance towards H_2O_2 electroreduction. Generally, noble metal electrocatalysts are supported on various carbon materials including carbon black,[19] mesoporous carbon,[20] carbon nanotubes,[21] and graphene,[22] which can supply enough surface area for catalyst loading and excellent electrical conductivity for charge transfer. More recently, metal substrates have also been employed to support these electrocatalysts owing to the improved performance capabilities that result from improved interactions between the substrates and the catalysts.[23,24] It has been suggested that metal substrates with large surface areas, high conductivity and excellent chemical stability can provide much enhanced catalytic properties.

Meanwhile, highly porous metals and composites have been studied as electrocatalysts to demonstrate superior performances.[25–28] Among them, nanoporous gold (NPG) has attracted significant research interest owing to its stable bicontinuous structure consisting of both solid ligaments and empty channels.[29] Unlike many other nanoporous materials, NPG exhibits excellent conductivity, structural continuity, mechanical and chemical stability, along with several other unique properties that make it promising for numerous applications in heterogeneous catalysis,[30] supercapacitors,[31] actuators[32] and surface-enhanced Raman scattering (SERS).[33] Furthermore, NPG films can be employed as both electrocatalysts and current collectors for electrochemical reactions owing to their high catalytic activity coupled with bulk scale electrical conductivity.

In this work, we design and prepare a new type of three-dimensional (3D) hierarchical porous electrode using NPG/Ni foam to support well-dispersed Pd nanoparticles through a facile

[a]Electronic Packaging Electrochemistry Laboratory, School of Chemistry and Chemical Engineering, Sun Yat-sen University, Guangzhou, 510275, China. E-mail: cuigf@mail.sysu.edu.cn

[b]School of Mechanical and Automotive Engineering, South China University of Technology, Guangzhou, 510640, China

[c]Materials Physics and Applications Division, Los Alamos National Laboratory, Los Alamos, New Mexico 87545, USA

[d]Department of Chemical Engineering, University of Waterloo, Waterloo, Ontario N2L 3G1, Canada

[e]Department of Chemical and Biological Engineering, University at Buffalo, The State University of New York, Buffalo, New York 14260, USA

three-step procedure. Specifically, the NPG film was firstly fabricated on a Ni foam substrate by electrodeposition of an Au–Sn alloy film, followed by selective leaching of the Sn component using a chemical dealloying process. Pd nanoparticles were then deposited on the NPG/Ni foam electrode by a potentiostatic electrodeposition method. Taking advantage of its hierarchical porous structure and large surface area, the NPG/Ni foam can provide excellent Pd nanoparticle dispersion. The morphology of the Pd-decorated NPG/Ni foam (Pd@NPG/Ni foam) composite electrode was determined. This unique structure is then investigated as a standalone electrode for electrocatalytic activity towards H_2O_2 electroreduction in acid media and was found to provide excellent performance towards H_2O_2 electroreduction in acid media.

2. Experimental

2.1. Preparation of Pd@NPG/Ni foam electrode

The preparation of the Pd@NPG/Ni foam composite electrode involves a three-step procedure. Firstly, an Au–Sn alloy film was synthesized on Ni foam by an electrodeposition process.[34] Typically, Ni foam (10 mm × 60 mm) with a thickness of 1 mm (Changsha Lyrun Material Co., Ltd., China) was pretreated with 5 M HCl solution, absolute ethanol, and deionized water step by step for 30 min for each treatment in order to clean and activate the surface. Then the Au–Sn alloy deposition was conducted in a two-electrode electrochemical cell. The Ni foam was used as the cathode and platinum foil was used as the anode. The Au–Sn alloy film was electrodeposited from a plating solution (Huizhou Leadao Electronic Materials Co., Ltd., China, webpage: http://www.leadao.cn) by applying a constant current density of 0.5 A dm^{-2} for 300 s. After the deposition, the electrode was removed from the solution, rinsed with deionized water thoroughly and dried in air. Secondly, the NPG films on the Ni foam were produced by chemical dealloying of the Au–Sn alloy that was already deposited onto Ni foam. Specifically, the Au–Sn alloy deposited Ni foam was immersed into an aqueous solution of 5 M NaOH + 1 M H_2O_2 for 3 days under spontaneous corrosion conditions. After the dealloying process, the electrode was removed from the solution, rinsed with deionized water thoroughly and dried in air. Finally, Pd nanoparticles were electrodeposited on the NPG/Ni foam electrode from an aqueous solution containing 1 mM K_4PdCl_6 (Sigma-Aldrich) and 0.1 M HCl by a potentiostatic electrodeposition method. The Pd electrodeposition experiments were performed in a standard three-electrode electrochemical cell. The NPG/Ni foam electrode was used as the working electrode, platinum foil as the counter electrode and a saturated calomel electrode (SCE) as the reference electrode. All potentials reported in this work were referenced to the SCE reference electrode. The Pd electrodeposition was conducted by applying a constant potential at −0.6 V for 300 s. Then, the electrode was removed from the solution, rinsed with deionized water thoroughly and dried in air.

2.2. Physical characterization of Pd@NPG/Ni foam electrode

The morphology of the composite electrode was characterized using a scanning electron microscope (SEM, JEOL, JSM-6700F, 15 KeV). The content of Au and Pd in the Pd@NPG/Ni foam composite electrode was determined using an inductively coupled plasma atomic emission spectrometer (ICP-AES, ICAP 6500 Duo, Thermo Scientific). Au and Pd contents on the Pd@NPG/Ni foam composite electrode were found to be 2.93 mg cm^{-2} and 0.35 mg cm^{-2}, respectively.

2.3. Electrochemical measurements

Cyclic voltammetry (CV), linear scan voltammetry (LSV), chronoamperometry (CA), and electrochemical impedance spectroscopy (EIS) were performed in a conventional three-electrode electrochemical cell using a potentiostat (Gamry REF 600 Electrochemical Workstation). NPG/Ni foam or Pd@NPG/Ni foam composite electrodes (1 cm^2 geometrical area) were used as the working electrodes. Platinum foil and an SCE were employed as the counter and reference electrodes, respectively. All electrochemical measurements were conducted at room temperature. The electrolyte was 0.5 M H_2SO_4 solution. All solutions were prepared with analytical grade chemical reagents and double-distilled water (18 MΩ cm). EIS measurements were performed by applying an AC voltage with 5 mV amplitude in a frequency range from 100 kHz to 0.01 Hz.

3. Results and discussion

The design and facile preparation of the Pd@NPG/Ni foam composite electrode are schematically illustrated in Fig. 1. At first, Au–Sn alloy films were electrodeposited onto the 3D Ni foam surface. Secondly, the as-prepared Au–Sn alloy film was subjected to a chemically dealloying process to remove Sn in order to prepare NPG layers on the Ni foam substrate. Thirdly, the NPG/Ni foam was used as a substrate for subsequent growth of Pd nanoparticles through an electrodeposition approach. As compared in Fig. 2, we have systematically studied the morphology changes during the electrode preparation step by step. Specifically, Fig. 2A and B show the SEM images of the Ni foam used in this work, indicating a 3D porous and cross-linked skeleton structure with a smooth surface. Fig. 2C and D display the SEM images of electrodeposited Au–Sn alloy films onto the Ni foam. It can be seen that the Ni foam surface is fully covered with Au–Sn alloy grains with a size range of 50–300 nm. Subsequently, the images for chemically dealloyed NPG films

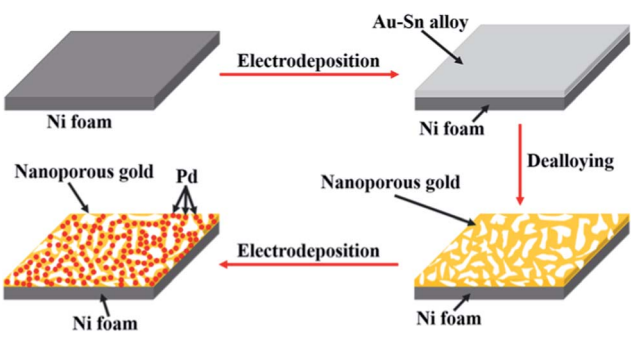

Fig. 1 Scheme of the preparation procedure of a Pd@NPG/Ni foam composite electrode.

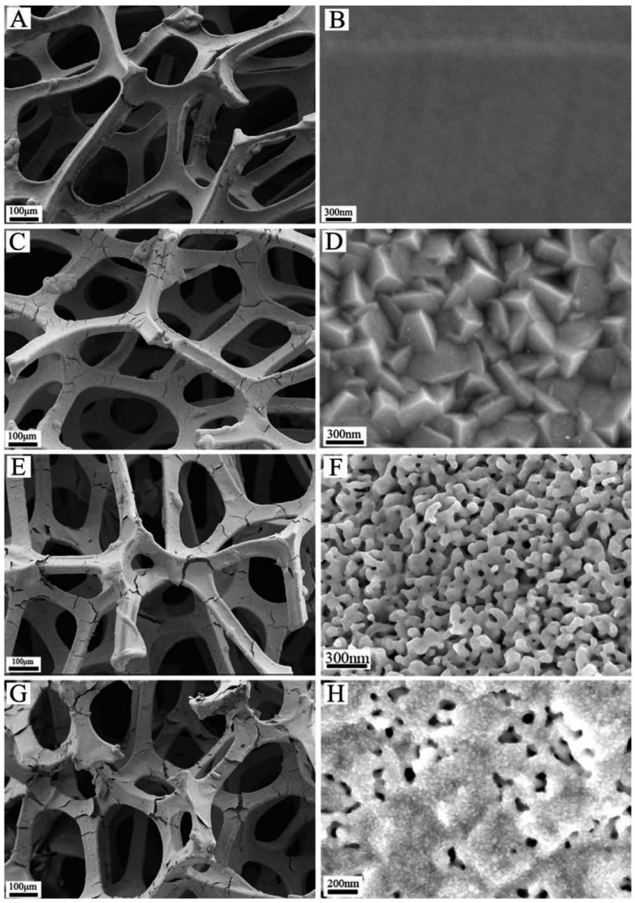

Fig. 2 SEM images of (A and B) the as-obtained Ni foam at different magnifications, (C and D) the Au–Sn alloy films deposited on the Ni foam surface at different magnifications, (E and F) the NPG films resulted from dealloying of Au–Sn films, and (G and H) the Pd nanoparticles well dispersed on the NPG/Ni foam composite electrodes at different magnifications.

on Ni foam are shown in Fig. 2E and F, presenting a sponge-like film morphology. Especially, the high-magnification SEM image (Fig. 2F) reveals that the NPG film consists of bicontinuous nanostructures with interconnected ligaments and nanopores. The ligament size is about 50–100 nm and the pore size is about 30–90 nm. Such 3D micro/nanopore integrated electrode structures are able to be beneficial for enhancing electrochemical reaction rates, due to short mass transfer lengths allowing liquid and gas species reacting at the electrode/electrolyte interface efficiently. Moreover, the framework can accommodate high catalyst loadings due to its large surface area resulting from the hierarchical porous structure. More importantly, the coated NPG film could provide a robust protection layer on the Ni foam that is traditionally unstable in acidic solutions. Furthermore, the Pd nanoparticles were deposited using a simple and reproducible electrodeposition route. Fig. 2G and H display SEM images for the Pd deposited NPG/Ni foam electrode. Numerous Pd nanoparticles are densely and uniformly packed on the NPG skeleton and the nanoporous structure was retained after the Pd electrodeposition. The corresponding energy dispersive X-ray spectroscopy (EDX) and elemental mapping results for the Pd@NPG/Ni foam composite electrode are shown in Fig. 3. The EDX result (Fig. 3A) confirmed the existence of Ni, Au and Pd. Meanwhile, the EDX elemental mapping (Fig. 3B–D) further demonstrated the uniform distribution of Pd nanoparticles on the NPG/Ni foam skeleton.

Fig. 4 shows the CVs of NPG/Ni foam and Pd@NPG/Ni foam electrodes in 0.5 M H_2SO_4 solution at a scan rate of 50 mV s^{-1}. A strong anodic peak at 1.2 V and a cathodic peak at 0.9 V appear for both electrodes due to typical responses of polycrystalline gold electrodes in acid solutions.[35] The oxidation and reduction peaks can be attributed to the formation and reduction of a surface gold oxide on the NPG materials, respectively, which is consistent with a previous report.[36] After deposition of Pd, the CV profile of the Pd@NPG/Ni foam electrode displays the hydrogen adsorption/desorption peaks and surface oxide formation/reduction peaks. These peaks represent the typical response of the polycrystalline Pd electrode in acid solution,[37] demonstrating that Pd was successfully deposited on the NPG/Ni foam electrode.

Fig. 5 shows a comparison for NPG/Ni foam, Pd@Ni foam, and Pd@NPG/Ni foam electrodes in terms of their catalytic activity toward the H_2O_2 electroreduction. Compared to NPG/Ni foam, Pd@Ni foam and Pd@NPG/Ni foam electrodes exhibit enhanced catalytic activity. The onset reduction potentials on the Pd@Ni foam and the Pd@NPG/Ni foam electrodes are around 0.5 V, approximately 0.2 V higher than that on the NPG/Ni foam electrode. At 0 V, a high reduction current density of 178 mA cm^{-2} was achieved on the Pd@NPG/Ni foam electrode in comparison to 98 mA cm^{-2} on the Pd@Ni foam electrode and 36 mA cm^{-2} on the NPG/Ni foam electrode. These results indicate that Pd decoration of the NPG/Ni foam electrode effectively improves its catalytic activity toward the H_2O_2 electroreduction in acid media. As the bare Ni foam electrode is rapidly dissolved into the acidic electrolyte during the polarization test, deposition of NPG onto Ni foam can significantly enhance the stability of Ni foam in the acidic environment during the electrochemical measurements, due to the superior electrochemical stability of Au. Therefore, the NPG films on Ni foam not only provide catalytic sites for the H_2O_2 reduction, but also prevent Ni foam substrates from oxidative corrosion. Importantly, the formation of NPG layers onto the Ni foam substrates leads to higher surface areas, thereby increasing the number of active sites for the H_2O_2 electroreduction.

Fig. 6 shows the effect of H_2O_2 concentration on the H_2O_2 electroreduction activity of the Pd@NPG/Ni foam composite electrode. The measured current densities increase significantly with an increase of H_2O_2 concentration from 0.2 to 0.8 M, while the further increase of H_2O_2 concentration to 1.0 M only leads to a slight increase of current density. It should be noted that the chemical decomposition of H_2O_2 became more significant with increasing H_2O_2 concentration, which would limit the reduction current density.

Fig. 7A shows the chronoamperometric curves for the H_2O_2 electroreduction on the Pd@NPG/Ni foam composite electrode measured in 0.5 M H_2SO_4 + 0.6 M H_2O_2. The current density measured at 0.4 V is very stable, indicating that the Pd@NPG/Ni

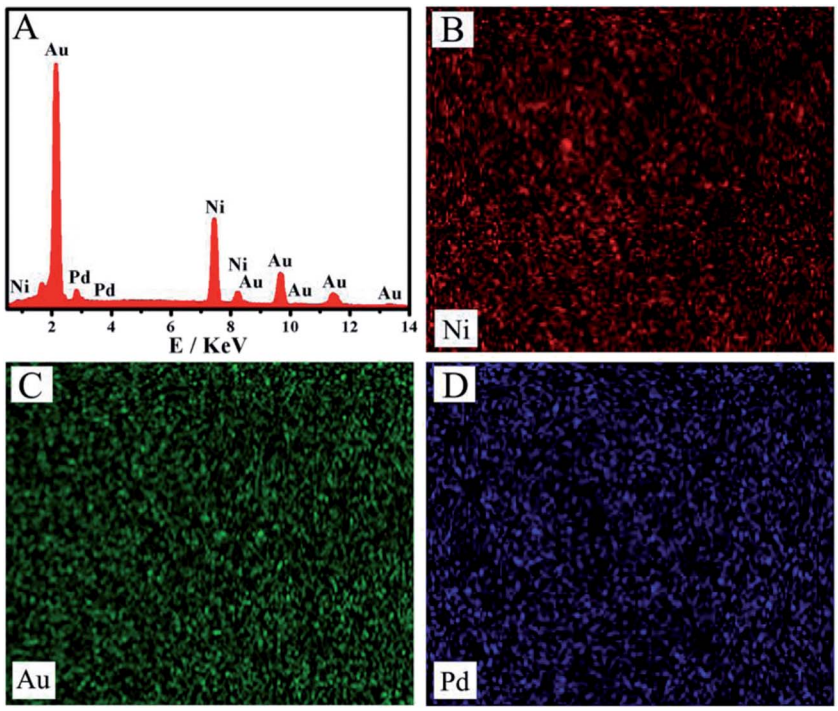

Fig. 3 (A) EDX and elemental mapping of (B) Ni, (C) Au and (D) Pd of the Pd@NPG/Ni foam composite electrode.

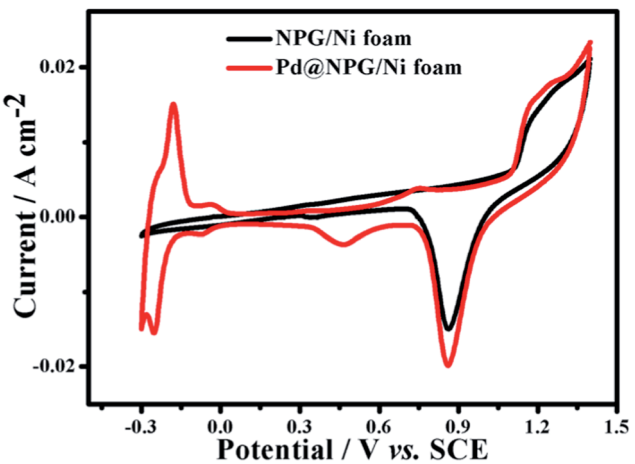

Fig. 4 Cyclic voltammograms of the NPG/Ni foam electrode and the Pd@NPG/Ni foam electrode in 0.5 M H_2SO_4 solution at a scan rate of 50 mV s^{-1}.

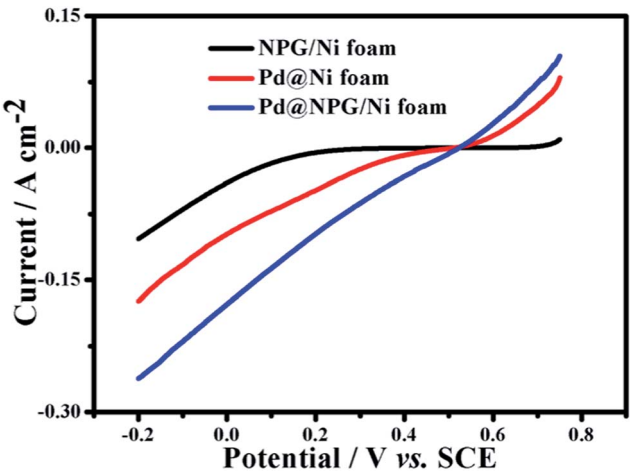

Fig. 5 Polarization plots for H_2O_2 electroreduction at the NPG/Ni foam electrode, the Pd@Ni foam electrode and the Pd@NPG/Ni foam electrode in 0.5 M H_2SO_4 + 0.6 M H_2O_2 at a scan rate of 5 mV s^{-1}.

foam electrode exhibits excellent stability for the H_2O_2 electroreduction in acid media. However, the gradually decreased current densities were observed at 0.3 V and 0.2 V, which may be ascribed to the decrease of H_2O_2 concentration at the electrode surface resulting from the fast reduction rate at more negative potentials. Additionally, in order to further evaluate the stability of Pd@NPG/Ni foam, accelerated degradation tests through potential cycling between 0.75 V and −0.2 V were conducted on the Pd@NPG/Ni foam electrode in 0.5 M H_2SO_4 + 0.6 M H_2O_2. As shown in Fig. 7B, the Pd@NPG/Ni foam electrode demonstrated excellent stability with negligible loss in current density after 4000 cycles.

Fig. 8 displays the EIS results of the NPG/Ni foam and Pd@NPG/Ni foam electrodes measured in 0.5 M H_2SO_4 + 0.6 M H_2O_2. The measured spectra display a semicircle spanning the high and low frequency regions for both the NPG/Ni foam and the Pd@NPG/Ni foam electrodes. However, the diameter of the semicircle for the Pd@NPG/Ni foam electrode was much smaller than that of the NPG/Ni foam, demonstrating that the charge transfer rate on the Pd@NPG/Ni foam electrode is much faster than that on the NPG/Ni foam. The experimental data are further simulated using an equivalent circuit that is composed of a constant phase element (CPE)/resistive element and a

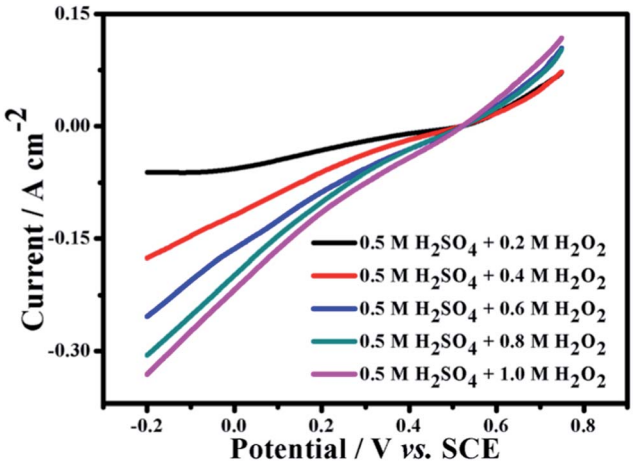

Fig. 6 Polarization plots for H_2O_2 electroreduction at the Pd@NPG/Ni foam composite electrode in 0.5 M H_2SO_4 as a function of addition of different concentrations of H_2O_2 at a scan rate of 5 mV s^{-1}.

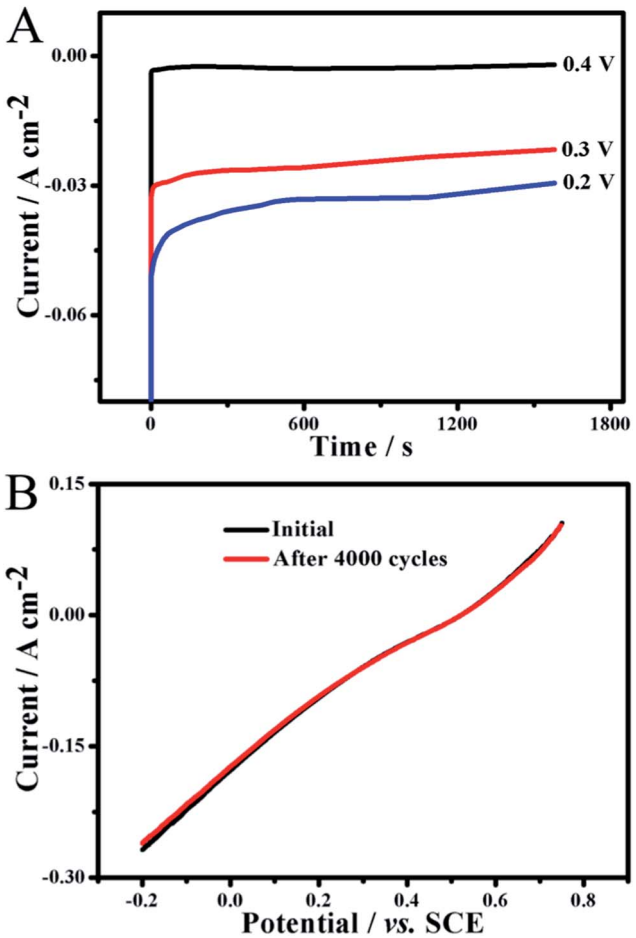

Fig. 7 (A) Chronoamperometric curves for H_2O_2 electroreduction on the Pd@NPG/Ni foam composite electrode at different potentials in 0.5 M H_2SO_4 + 0.6 M H_2O_2. (B) Polarization plots for the Pd@NPG/Ni foam composite electrode in 0.5 M H_2SO_4 + 0.6 M H_2O_2 at a scan rate of 5 mV s^{-1} before and after 4000 cycles at a scan rate of 100 mV s^{-1} between 0.75 V and −0.2 V.

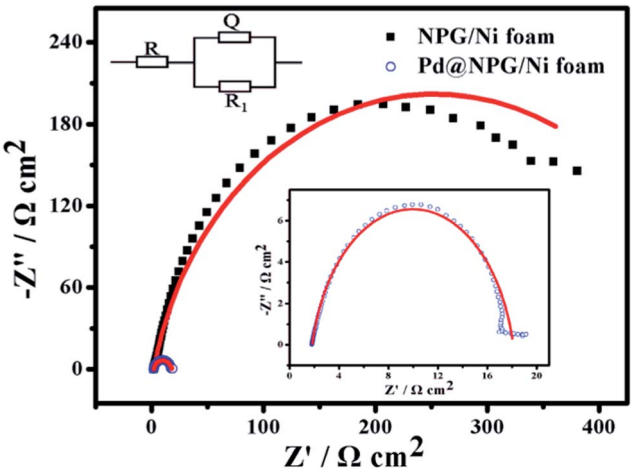

Fig. 8 Electrochemical impedance spectra (EIS) of the NPG/Ni foam and the Pd@NPG/Ni foam electrode measured in 0.5 M H_2SO_4 + 0.6 M H_2O_2. Scattered symbols: experimental data. Solid lines: simulated results. The inset at the below is the zoom-in of the EIS spectra of the Pd@NPG/Ni foam electrode. The inset at the top left is the equivalent circuit employed to simulate the experimental results.

resistance in series (Fig. 8, top left inset). The simulation results (solid line) fitted well with the experimental results (symbols). R is the ohmic resistance resulting from the electrode and the electrolyte. R_1 is the charge transfer resistance of the H_2O_2 electroreduction. Q is the corresponding constant phase angle element. According to the simulation, the values of R are 2.1 and 1.8 Ω cm^2 for the NPG/Ni foam and the Pd@NPG/Ni foam electrodes, respectively. The value of R_1 for the Pd@NPG/Ni foam electrode (16.3 Ω cm^2) is much smaller than that for the NPG/Ni foam electrode (502 Ω cm^2), suggesting that the charge transfer during the H_2O_2 electroreduction over Pd@NPG/Ni foam electrode is much faster than that of NPG/Ni foam, which is in good agreement with the results depicted in Fig. 5.

4. Conclusions

In this work, Ni foam deposited with a nanoporous gold film was employed as a conductive solid 3D porous support to load Pd nanoparticles *via* a facile electrodeposition approach, which was developed as an efficient catalyst for electrocatalytic H_2O_2 reduction. The NPG film deposited on Ni foams is able to provide robust protection and efficiently increase its stability in acid media. The Pd decoration plays an important role in significantly enhancing the catalytic activity of the NPG/Ni foam electrode toward the H_2O_2 electroreduction. The Pd@NPG/Ni foam composite electrode exhibited the highest current density of 178 mA cm^{-2} at 0 V in 0.5 M H_2SO_4 + 0.6 M H_2O_2 electrolytes, compared to NPG/Ni foam and Pd/Ni foam electrodes. Furthermore, the Pd@NPG/Ni foam electrode demonstrated an excellent stability for the H_2O_2 electroreduction in acid media. The high electrochemical performance is attributed to the 3D hierarchical porous structure and well-dispersed Pd nanoparticles onto NPG/Ni foam, thereby resulting in efficient mass and charge transfer during the H_2O_2 electroreduction. The

newly developed Pd@NPG/Ni foam composite electrode through a facile fabrication protocol holds great promise for the applications in borohydride–H_2O_2 and hydrazine–H_2O_2 fuel cell technologies.

Acknowledgements

G.F.C. gratefully acknowledges the financial support by the National Natural Science Foundation of China (51271205, 50801070), "The Fundamental Research Funds for the Central Universities" (11lgpy08), "Guangzhou Pearl Technology the Nova Special Project" (2012J2200058), "Research and Application of Key Technologies Oriented the Industrial Development" (90035-3283309), "Plan of Science and Technology Project" by the DaYa Gulf district in Huizhou city (31000-4207387), the Innovative Laboratory Fund by Sun Yat-sen University and the Foundation for Distinguished Young Teachers in Higher Education of Guangdong, China (Yq2013006). G.W. is grateful to the start-up fund of SUNY Buffalo.

References

1 D. M. F. Santos, P. G. Saturnino, R. F. M. Lobo and C. A. C. Sequeira, *J. Power Sources*, 2012, **208**, 131.
2 X. L. Yan, F. H. Meng, Y. Xie, J. G. Liu and Y. Ding, *Sci. Rep.*, 2012, **2**, 941.
3 D. X. Cao, D. D. Chen, J. Lan and G. L. Wang, *J. Power Sources*, 2009, **190**, 346.
4 F. Yang, K. Cheng, Y. H. Mo, L. Q. Yu, J. L. Yin, G. L. Wang and D. X. Cao, *J. Power Sources*, 2012, **217**, 562.
5 A. L. Morais, J. R. C. Salgado, B. Sljukic, D. M. F. Santos and C. A. C. Sequeira, *Int. J. Hydrogen Energy*, 2012, **37**, 14143.
6 K. Cheng, F. Yang, D. M. Zhang, J. L. Yin, D. X. Cao and G. L. Wang, *Electrochim. Acta*, 2013, **105**, 115.
7 X. Li, D. Heryadi and A. A. Gewirth, *Langmuir*, 2005, **21**, 9251.
8 D. X. Cao, Y. Y. Gao, G. L. Wang, R. R. Miao and Y. Liu, *Int. J. Hydrogen Energy*, 2010, **35**, 807.
9 J. S. Jirkovsky, M. Halasa and D. J. Schiffrin, *Phys. Chem. Chem. Phys.*, 2010, **12**, 8042.
10 X. Qin, Z. Y. Miao, Y. X. Fang, D. Zhang, J. Ma, L. Zhang, Q. Chen and X. G. Shao, *Langmuir*, 2012, **28**, 5218.
11 T. C. Nagaiah, D. Schafer, W. Schuhmann and N. Dimcheva, *Anal. Chem.*, 2013, **85**, 7897.
12 F. Yang, K. Cheng, T. H. Wu, Y. Zhang, J. L. Yin, G. L. Wang and D. X. Cao, *J. Power Sources*, 2013, **233**, 252.
13 K. Cheng, D. X. Cao, F. Yang, Y. Xu, G. H. Sun, K. Ye, J. L. Yin and G. L. Wang, *J. Power Sources*, 2014, **253**, 214.
14 G. L. Wang, D. X. Cao, C. L. Yin, Y. Y. Gao, J. L. Yin and L. Cheng, *Chem. Mater.*, 2009, **21**, 5112.
15 Y. H. Li, D. X. Cao, Y. Liu, R. Liu, F. Yang, J. L. Yin and G. L. Wang, *Int. J. Hydrogen Energy*, 2012, **37**, 13611.
16 K. Cheng, F. Yang, G. L. Wang, J. L. Yin and D. X. Cao, *J. Mater. Chem. A*, 2013, **1**, 1669.
17 K. Cheng, F. Yang, Y. Xu, L. Cheng, Y. Y. Bao, D. X. Cao and G. L. Wang, *J. Power Sources*, 2013, **240**, 442.
18 G. L. Wang, Y. Y. Bao, Y. M. Tian, J. Xia and D. X. Cao, *J. Power Sources*, 2010, **195**, 6463.
19 M. Carmo, A. R. Dos Santos, J. G. R. Poco and M. Linardi, *J. Power Sources*, 2007, **173**, 860.
20 Z. X. Yan, M. M. Zhang, J. M. Xie, H. E. Wang and W. Wei, *J. Power Sources*, 2013, **243**, 48.
21 B. Liu, H. Y. Li, L. Die, X. H. Zhang, Z. Fan and J. H. Chen, *J. Power Sources*, 2009, **186**, 62.
22 H. Gu, Y. Yang, J. X. Tian and G. Y. Shi, *ACS Appl. Mater. Interfaces*, 2013, **5**, 6762.
23 J. L. Zhang, M. B. Vukmirovic, Y. Xu, M. Mavrikakis and R. R. Adzic, *Angew. Chem., Int. Ed.*, 2005, **44**, 2132.
24 J. Y. Liu, *ChemCatChem*, 2011, **3**, 934.
25 Y. Xu and B. Zhang, *Chem. Soc. Rev.*, 2014, **43**, 2439.
26 Y. Xu, S. X. Hou, Y. Liu, Y. Zhang, H. Wang and B. Zhang, *Chem. Commun.*, 2012, **48**, 2665.
27 Y. Xu, R. Xu, J. H. Cui, Y. Liu and B. Zhang, *Chem. Commun.*, 2012, **48**, 3881.
28 S. Xiao, F. Xiao, Y. Hu, S. L. Yuan, S. Wang, L. H. Qian and Y. Q. Liu, *Sci. Rep.*, 2014, **4**, 4370.
29 J. Erlebacher, M. J. Aziz, A. Karma, N. Dimitrov and K. Sieradzki, *Nature*, 2001, **410**, 450.
30 A. Wittstock, V. Zielasek, J. Biener, C. M. Friend and M. Baumer, *Science*, 2010, **327**, 319.
31 X. Y. Lang, A. Hirata, T. Fujita and M. W. Chen, *Nat. Nanotechnol.*, 2011, **6**, 232.
32 E. Detsi, P. Onck and J. T. M. De Hosson, *ACS Nano*, 2013, **7**, 4299.
33 L. Zhang, X. Y. Lang, A. Hirata and M. W. Chen, *ACS Nano*, 2011, **5**, 4407.
34 X. Ke, Y. T. Xu, C. C. Yu, J. Zhao, G. F. Cui, D. Higgins, Q. Li and G. Wu, *J. Power Sources*, 2014, **269**, 461.
35 L. D. Burke and A. P. O'Mullane, *J. Solid State Electrochem.*, 2000, **4**, 285.
36 R. Zeis, T. Lei, K. Sieradzki, J. Snyder and J. Erlebacher, *J. Catal.*, 2008, **253**, 132.
37 R. Pattabiraman, *Appl. Catal., A*, 1997, **153**, 9.